Journal of Biomechanics 69 (2018) 113–120

Contents lists available at ScienceDirect

Journal of Biomechanics

journal homepage: www.elsevier.com/locate/jbiomech
www.JBiomech.com

Hip chondrolabral mechanics during activities of daily living: Role of the labrum and interstitial fluid pressurization

Jocelyn N. Todd [a], Travis G. Maak [b], Gerard A. Ateshian [c], Steve A. Maas [a], Jeffrey A. Weiss [a,b,*]

[a] Department of Bioengineering, and Scientific Computing and Imaging Institute, University of Utah, Salt Lake City, UT 84112, United States
[b] Department of Orthopedics, University of Utah, Salt Lake City, UT 84108, United States
[c] Department of Mechanical Engineering, Columbia University, New York, NY 10027, United States

ARTICLE INFO

Article history:
Accepted 8 January 2018

Keywords:
Hip
Cartilage mechanics
Labrum
Biphasic
Finite element

ABSTRACT

Osteoarthritis of the hip can result from mechanical factors, which can be studied using finite element (FE) analysis. FE studies of the hip often assume there is no significant loss of fluid pressurization in the articular cartilage during simulated activities and approximate the material as incompressible and elastic. This study examined the conditions under which interstitial fluid load support remains sustained during physiological motions, as well as the role of the labrum in maintaining fluid load support and the effect of its presence on the solid phase of the surrounding cartilage. We found that dynamic motions of gait and squatting maintained consistent fluid load support between cycles, while static single-leg stance experienced slight fluid depressurization with significant reduction of solid phase stress and strain. Presence of the labrum did not significantly influence fluid load support within the articular cartilage, but prevented deformation at the cartilage edge, leading to lower stress and strain conditions in the cartilage. A morphologically accurate representation of collagen fibril orientation through the thickness of the articular cartilage was not necessary to predict fluid load support. However, comparison with simplified fibril reinforcement underscored the physiological importance. The results of this study demonstrate that an elastic incompressible material approximation is reasonable for modeling a limited number of cyclic motions of gait and squatting without significant loss of accuracy, but is not appropriate for static motions or numerous repeated motions. Additionally, effects seen from removal of the labrum motivate evaluation of labral reattachment strategies in the context of labral repair.

1. Introduction

Osteoarthritis (OA) of the hip is a significant health issue, affecting 8% of the overall population (Dagenais et al., 2009). Mechanical factors are understood to influence the initiation and progression of the disease (Carter et al., 2004; Guilak, 2011; Guilak et al., 2004; Mankin, 1974) and have been readily studied using computational methods, especially finite element (FE) analysis. Modern FE solvers are equipped to handle increasingly complex constitutive models and geometries for more accurate predictions of joint mechanics and, specifically, more relevant insight into potential risk factors for OA development (Ateshian et al., 2015). In particular, articular cartilage is often represented as a hydrated mixture of a solid phase and fluid phase, whose behavior is described by biphasic theory (Mow et al., 1980; Mow and Lai, 1980). The high level of hydration in articular cartilage is known to influence the mechanics of the tissue through fluid pressurization, and also functions as the dominant dissipative mechanism via flow-dependent viscoelasticity (Huang et al., 2001; Park et al., 2004). Nonetheless, FE studies in the hip often approximate articular cartilage as incompressible and elastic under the implicit assumption that there is no significant loss of fluid pressurization in cartilage of the hip during the simulated activities (Anderson et al., 2008; Anderson et al., 2010; Chegini et al., 2009; Henak et al., 2014a; Henak et al., 2014b; Henak et al., 2011; Liu et al., 2016). Although dimensional analysis suggests that this may be a reasonable assumption for some loading conditions (Ateshian et al., 2007; Li et al., 2014), the appropriate range of applicability for this assumption and the factors influencing its validity are not well understood.

Although computational studies have shown that the fluid phase of cartilage supports ~90% of loads during most activities in the hip (Li et al., 2014; Li et al., 2013; Pawaskar et al., 2011), it

* Corresponding author at: Department of Bioengineering, University of Utah, 72 South Central Campus Dr., Room 3750, Salt Lake City, UT 84112, United States.

E-mail addresses: Jocelyn.todd@utah.edu (J.N. Todd), Travis.maak@hsc.utah.edu (T.G. Maak), Ateshian@columbia.edu (G.A. Ateshian), Steve.maas@utah.edu (S.A. Maas), Jeff.weiss@utah.edu (J.A. Weiss).

https://doi.org/10.1016/j.jbiomech.2018.01.001
0021-9290/

is unclear how inclusion of the fluid phase affects stress and strain conditions in the solid phase, which are used to assess the risk of damage to the extracellular matrix (Bader et al., 2011; Carter et al., 2004; Grodzinsky et al., 2000; Guilak, 2011; Guilak et al., 2004). To ensure accurate predictions for the solid phase, it is critical to assess the contributions of the fluid phase before assuming the material can be represented as elastic and incompressible.

Experimental studies demonstrate the ability of the labrum to provide a seal to prevent fluid exudation from the joint space (Dwyer et al., 2015; Dwyer et al., 2014; Ferguson et al., 2003; Philippon et al., 2014) and it is suggested this mechanism also sustains fluid pressure within the cartilage layers of the hip (Dwyer et al., 2014; Ferguson et al., 2003). However, there are contradictory opinions on the role of the labrum in maintaining fluid load support within the articular cartilage (Dwyer et al., 2015; Ferguson et al., 2000a). Additionally, the potential influence of the labrum on the stress and strain conditions within the solid phase of the cartilage has not been extensively studied.

The primary objectives of this study were to determine the conditions under which interstitial fluid load support remains sustained during physiological motions, and to determine the role of the labrum in maintaining fluid load support in the articular cartilage of the hip and the effect of its presence on the solid phase of the surrounding cartilage. Additionally, the effect of varied fibril orientation through the thickness of the articular cartilage of the hip, the inclusion of strain-dependent and anisotropic permeability, as well as sensitivity of biphasic material parameters were determined. Transient mechanics of the solid and fluid phases of articular cartilage in a healthy, population-relevant, and idealized hip model were measured during single-leg stance, gait, and squatting.

2. Methods

2.1. Description of the finite element model

To obtain a computationally efficient model geometry that represented a normal population of hips in terms of radiographic measurements, a finite element model with idealized geometry was created. The model was based on the cartilage geometry of a representative normal hip (31 year old female, 60-kg, BMI 22 kg/m^2, center edge angle (CEA) 29.2°, acetabular index (AI) 9.7°), selected from a cohort of ten healthy patients from a previous study (five male and five female, BMI 23.0 ± 3.9 kg/m^2, age 26 ± 4 years, CEA 33.5 ± 5.4°, AI 7.6 ± 1.7°) (Fig. 1) (Harris et al., 2012). The articular surfaces of the femoral and acetabular cartilage were segmented from contrast enhanced CT data of the volunteer as part of the previous study. These surfaces representing the femoral and acetabular cartilage were fit to spheres and ellipsoids, respectively (Chegini et al., 2009; Macirowski et al., 1994). Comparison of the surfaces to metrics of average population geometry are described in Supplemental Methods section (Bergmann et al., 2001, Haemer et al., 2012). Surfaces representing the osteochondral boundaries were created by offsetting the articular surfaces based on average values for cartilage thickness in the hip according to the literature (femoral cartilage: 1.6 mm; acetabular cartilage: 1.5 mm) (Anderson et al., 2008; Liu et al., 2016; Shepherd and Seedhom, 1999). The geometry of the labrum was constructed by sweeping a cross-section of the labrum obtained from image data of the normal hip around the circumference of the acetabular cartilage geometry. Preprocessing, analysis, and postprocessing were performed using the FEBio software suite (www.febio.org) (Maas et al., 2016).

A baseline model was defined for subsequent comparisons. Material coefficients and material symmetry for the articular cartilage and labrum in the baseline model were chosen from information from the literature for the normal hip. The acetabular and femoral cartilage were represented as inhomogeneous, biphasic, anisotropic materials. Nonlinear behavior and tension-compression nonlinearity were represented with a continuous fiber distribution constitutive model embedded in a biphasic neo-Hookean ground matrix (shear modulus μ = 0.549 MPa, Poisson's ratio ν = 0.1) with fiber strain energy represented using a power law (initial fibril modulus ξ = 9.19 MPa, fiber power coefficient β = 4). The continuous fiber distribution captures tension-compression nonlinearity and strain-induced anisotropy of fibrils (Ateshian et al., 2009; Henak et al., 2014b). The chosen material coefficients for the ground matrix were fit to experimental data for biphasic creep indentation testing of human acetabular and femoral cartilage (Athanasiou et al., 1994) and the fibril properties were fit from unconfined compression of human acetabular cartilage (Henak et al., 2014b). The baseline model used a physiologically realistic variation of fibril orientation through the thickness of the cartilage (Minns and Steven, 1977), where the fibril modulus, ξ, was scaled continuously through the articular layer with fibril reinforcement aligned tangent to articular surface in superficial zone, homogenous in the middle zone, and perpendicular to the osteochondral interface in the deep zone (Fig. 2A). Additional information regarding specification of fibril orientation is provided in the Supplemental Methods section. The anisotropic strain-dependent permeability of the articular cartilage was represented using an anisotropic version of the Holmes-Mow constitutive equation ("perm-ref-ortho" in FEBio, radial permeability k_r = 4.475 × 10^{-4} mm^4/Ns, transchondral permeability k_z = 8.95 × 10^{-4} mm^4/Ns, exponential strain-dependent coefficient M = 15, power-law exponent α = 2) (Abraham et al., 2015; Athanasiou et al., 1994; Demarteau et al., 2006; Makela et al., 2012; Holmes and Mow, 1990; Wu and Herzog, 2000). This captures experimental findings that permeability is lower tangent to the articular surface (Reynaud and Quinn, 2006).

The labrum was represented as a biphasic, transversely-isotropic material consisting of a single fiber family embedded in an isotropic Mooney-Rivlin matrix ("coupled trans iso Mooney-Rivlin" material in FEBio, μ = 2.8 MPa, ν = 0.1, exponential toe region coefficients C_3 = 0.05 MPa and C_4 = 36, straightened fiber modulus C_5 = 66 MPa, fiber stretch for straightened fibers λ = 1.103) (Quapp and Weiss, 1998), with fiber reinforcement oriented

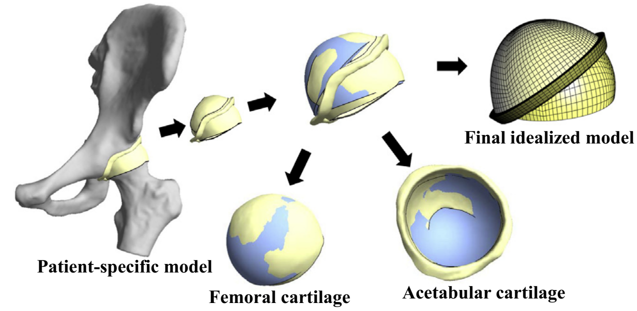

Fig. 1. The model for the current study was fit to cartilage geometry of a representative normal hip from a previous study (Harris et al., 2012). The surfaces representing the femoral and acetabular cartilage were fit to spheres and ellipsoids, respectively (Chegini et al., 2009; Macirowski et al., 1994) and the fit surfaces are shown in blue. Surfaces representing the osteochondral boundaries were created by offsetting the articular surfaces based on average values for cartilage thickness in the hip according to the literature (femoral cartilage: 1.6 mm; acetabular cartilage: 1.5 mm) (Anderson et al., 2008; Liu et al., 2016; Shepherd and Seedhom, 1999). The geometry of the labrum was constructed by sweeping a cross-section of the labrum obtained from image data of the normal hip around the circumference of the acetabular cartilage geometry. (For interpretation of the references to colour in this figure legend, the reader is referred to the web version of this article.)

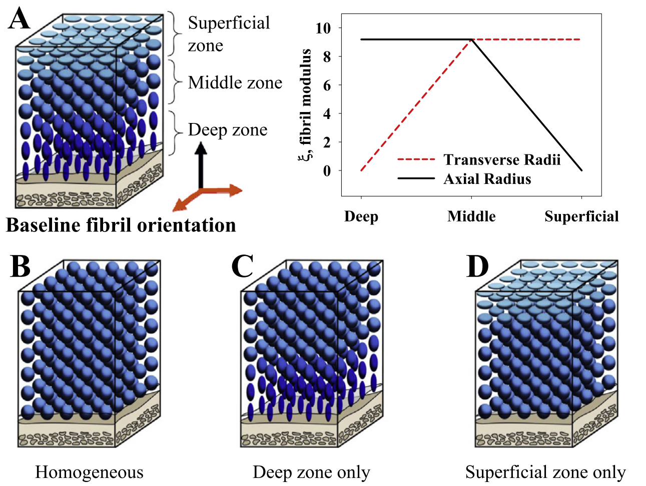

Fig. 2. The fibril orientation reported for articular cartilage was assigned by scaling the major and minor axes of the ellipsoids in the continuous fiber distribution model (Ateshian et al., 2009) according to the fibril contribution in that plane. The scaling of the axes was varied through the thickness of the layer to represent the gradient of fibril orientation: fibrils were oriented tangent to the surface in the superficial zone, spherical in the middle zone, and perpendicular to the osteochondral interface in the deep zone (Minns and Steven, 1977). The fibril orientation was simplified from (A) baseline to (B) homogeneous, (C) orientation in the deep zone only, and (D) orientation in the superficial zone only to assess its effects.

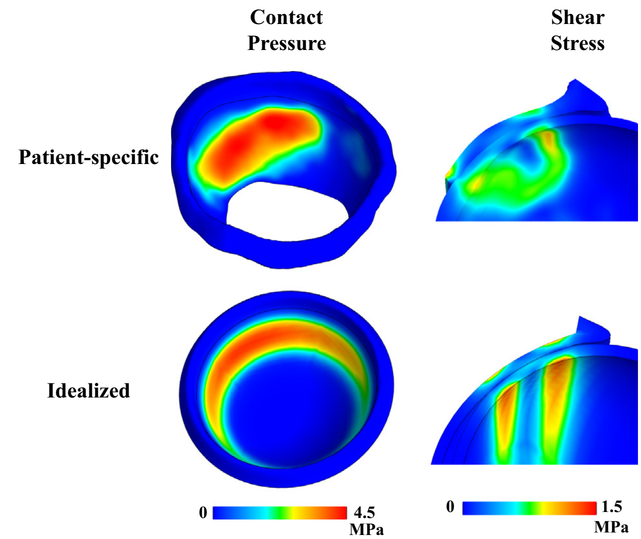

Fig. 3. The model for the current study was compared to population data to ensure relevant measures for size, thickness, curvature, and congruency. The resulting contact stress, contact area and maximum shear stress through the thickness of the idealized model compared well to the original, patient-specific model under physiological loading.

circumferentially around the acetabular rim, consistent with our previous studies (Henak et al., 2011; Klennert et al., 2017). Since pilot simulations showed that the labrum experienced very little strain and there are no available data for strain-dependent permeability of the labrum in the literature, permeability for the labrum was represented as constant and isotropic ("perm-const-iso" permeability type in FEBio, isotropic permeability $k = 0.0005\ mm^4/Ns$) (Ferguson et al., 2001).

Boundary conditions for all simulations and methods for the convergence study are described in the Supplemental Methods section. To assess the fidelity of the simplified model in comparison to a complete patient-specific model created in the previous study (Harris et al., 2012), we examined both models positioned the beginning of a gait cycle with an applied load of 78% body weight (533 N). The resulting predictions of contact pressure, contact area, and maximum shear stress through the thickness compared well to the native hip model (Fig. 3).

2.2. Sensitivity studies

Sensitivity analyses were performed to determine the relative influence of the biphasic constitutive representation (and thus fluid pressurization), the labrum, and baseline material coefficients on the transient mechanics of articular cartilage of the hip. The results of the baseline model were compared to models with different degrees of simplification and perturbations of the material definition. To assess the effects of fluid flow included in the simulation by representing articular cartilage as a biphasic material, the baseline model results were compared to an elastic, incompressible model. To assess the effect of the labrum on fluid phase in the cartilage and influence on the adjacent solid phase, it was removed and the resulting free surface at the edge of the articular cartilage was assigned a free-draining boundary condition. This removes any contribution from the labrum as a seal or boundary; fluid can flow out of the edge of the cartilage and deformation may occur at the edge if it was restricted by the stiffer, less permeable labrum. Additional sensitivity analyses are described in Supplemental Methods.

To assess the effects of the described simplifications on fluid pressurization, fluid load support (FLS) was calculated by integrating fluid pressure over the contact area on the articular surface and dividing it by the total force applied across the contact area (Ateshian and Wang, 1995). To investigate the effects of the simplifications on the mechanics of the solid phase of the articular cartilage, especially related to potential damage, peak tensile strain on the articular surface (E_1) and maximum shear stress at the osteochondral interface (τ_{max}) were evaluated as dependent variables. These quantities have been shown to lead to cartilage fissuring and delamination, respectively, and have been used previously to analyze mechanical conditions in the cartilage of the hip (Beck et al., 2005; Flachsmann et al., 1995; Henak et al., 2014a; Klennert et al., 2017).

3. Results

Over 90% of the load across the hip joint was initially supported by the fluid phase of articular cartilage during all three simulated activities of daily living (Fig. 4A, D, G). During single-leg stance (SLS) over the course of 600 s, fluid load support (FLS) decreased from 96% to 91% (Fig. 4A), while peak tensile strain at the articular surface (E_1) and maximum shear stress at the osteochondral interface (τ_{max}) both decreased by 12% and 47%, respectively (Fig. 4B, C). The model reached equilibrium conditions in the solid phase around 450 s, with $E_1 = 9\%$ and $\tau_{max} = 0.6$ MPa. During the cyclic activities of gait and squatting over 10 cycles, there was less than 1% decrease in FLS at peak loading (Fig. 4D, G), about 10% increase in E_1, and 12% relaxation in τ_{max} during gait with no change during squatting (Fig. 4E, F, H, I). Peak fluid pressure during SLS, gait, and squatting was 4.2, 5.5, and 4.9 MPa, respectively. A video displaying the simulated motions, as well as fluid pressure over time, is included in the Supplemental Material.

To assess any possible change in the predictions during longer term cyclic loading, an analysis of gait was repeated for 100 cycles. FLS at peak loading decreased slightly, from 95.6% to 94% (Fig. 5A). E_1 increased to roughly 13.5% strain at maximum loading, where it remained after about 60 cycles (Fig. 5B). τ_{max} also reach a steady peak value around 60 cycles, at approximately 0.9 MPa (Fig. 5C).

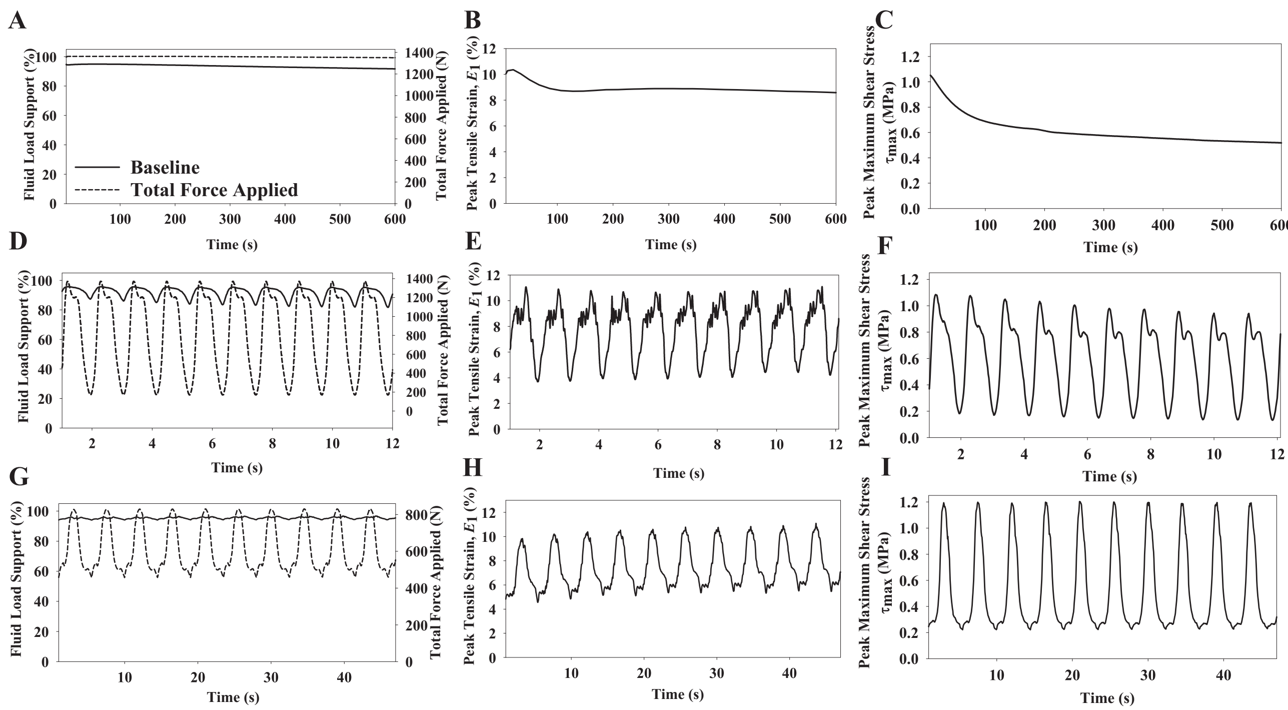

Fig. 4. Baseline model results during (A–C) single-leg stance (SLS) over 600 s, (D–F) gait over 10 cycles, and (G–I) squatting over 10 cycles. The dashed line in the first column of figures represents magnitude of total force applied to the joint for each activity and the solid line indicates the result over time. Fluid load support (FLS) is calculated as the ratio of total fluid force to total contact force on the articular surface of the cartilage. Tensile strain (1st principal strain), or E_1, was probed on the articular surface at the center of contact pressure during SLS and the center of contact at peak loading for gait and squatting. Similarly, maximum shear stress, or τ_{max}, was probed on the osteochondral interface during SLS and at peak loading for gait and squatting. While FLS decreases and E_1 and τ_{max} relax during 600 s of SLS, these variables remain consistent during 10 cycles of gait and squatting.

Removal of the labrum, which allowed fluid to drain freely from the outer edge of the acetabular cartilage, increased loss of FLS only slightly from baseline during the simulated 600 s of SLS; however, the lack of the labrum resulted in decreased relaxation of E_1 and τ_{max} during SLS compared to the baseline model (Fig. 6A). This was due to increased displacement of the cartilage edge at the articular surface (Fig. 7). During gait and squatting, removal of the labrum resulted in negligible changes to FLS, E_1, and τ_{max} compared to baseline values (Fig. 6B, C).

The incompressible elastic model experienced no change in τ_{max} or E_1 during SLS and experienced insignificant changes between peak loading of gait and squatting (Fig. 6). The consideration of the fluid phase in the baseline model resulted in large differences in E_1 and τ_{max} when compared to the elastic model; by −6.5% and 133%, respectively. At peak loading during gait and squatting, values of E_1 were within 1.5% strain and τ_{max} values were within 0.2 MPa between baseline and elastic models.

Results of the additional sensitivity studies regarding fibril orientation, permeability constitutive model, and biphasic material parameters are described in the Supplemental Results section.

4. Discussion

Compared to the elastic model, the representation of articular cartilage in the hip using a biphasic constitutive model had a large effect on the response of the solid phase during SLS, while the effect was minor during the dynamic motions of gait and squatting. This demonstrates that the mechanics of articular cartilage in the normal hip during similar dynamic, cyclic activities of daily living may be approximated with an elastic representation. The lack of variation of FLS between cycles during gait and squatting, in contrast to the depressurization during SLS, is consistent with theoretical studies demonstrating that motion between biphasic layers helps maintain high interstitial fluid pressure (Ateshian and Wang, 1995; Pawaskar et al., 2007). However, minimal depressurization during any of the conditions, especially considering the lack of re-balancing or slight loading/unloading included during the largest depressurization which occurred 600 s of SLS, suggests FLS within the cartilage layers is maintained during activities of daily living in hips with normal anatomy.

For all motions, the initial (time zero) fluid and solid phase results were identical between baseline and elastic cases. This is expected due to the intrinsic incompressibility of the solid and fluid phases, which creates a time at which biphasic simulations can be modeled as an incompressible and elastic solid (Ateshian et al., 2007; Bachrach et al., 1998; Carter and Beaupre, 1999; Eberhardt et al., 1990; Hayes et al., 1972). Ateshian et al proposed a time increment δt, during which this assumption is valid, that can be estimated (Ateshian et al., 2007) from:

$$\delta t \ll \frac{\Delta^2}{\|\mathbf{C}\|\|\mathbf{K}\|} \tag{1}$$

where Δ is the characteristic length, $\|\mathbf{C}\|$ is the Euclidian norm of the 4th order elasticity tensor, and $\|\mathbf{K}\|$ is the Euclidian norm of the 2nd order permeability tensor. For the current study, the characteristic length, Δ, was 12.2 mm and determined by measuring the height of the center of the contact band. Using $\|\mathbf{C}\| \sim 51$ MPa from the baseline model and $\|\mathbf{K}\| = 0.00175$ mm^4/Ns, a time increment of 3200 s can be found for the baseline model using Eq. (1). The findings of the present study provide a point of reference for interpreting this time increment, which is chosen similarly to a penalty factor to enforce an incompressible response. Since loss of FLS during SLS caused significant relaxation of articular tensile strain and maximum shear stress compared to the elastic model at less than 10 s, the time increment for modeling similar static scenarios

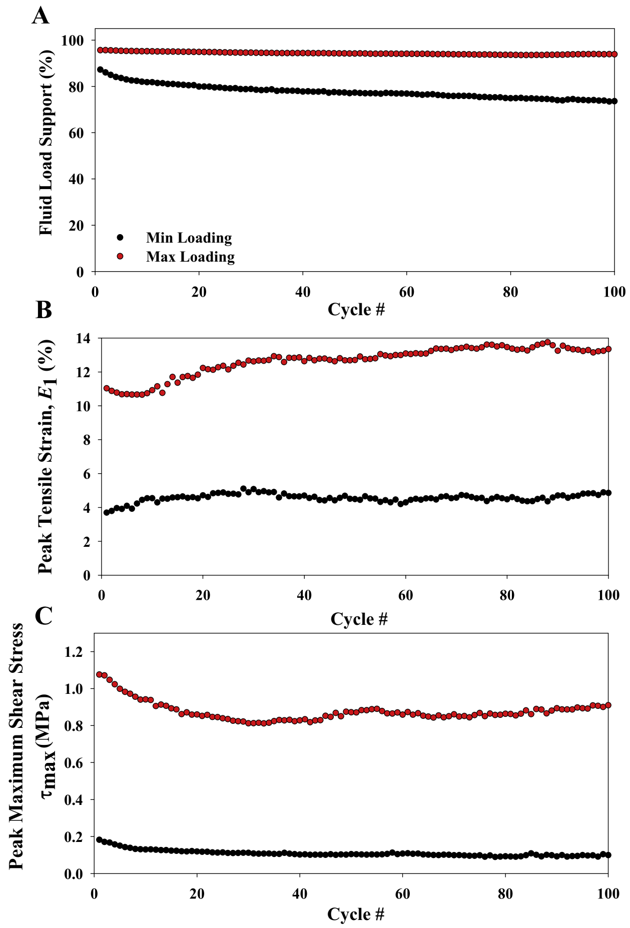

Fig. 5. One hundred cycles of gait were simulated to assess continued trends during minimum and maximum loading. (A) There was little change in fluid load support over time for the maximum and minimum loading of each loading cycle. (B) Tensile strain at maximum loading increased to roughly 13–13.7% strain, where it remained after about 60 cycles. (C) Maximum shear stress on the osteochondral interface decreased to an equilibrium value of approximately 0.9 MPa after about 60 cycles.

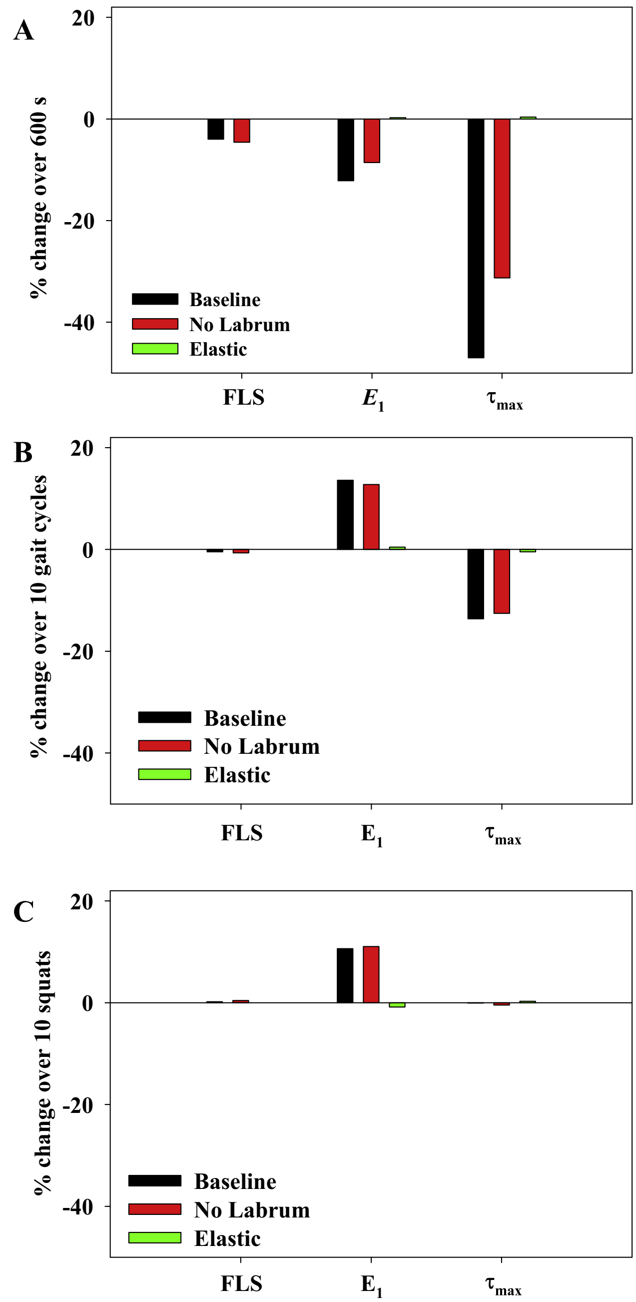

Fig. 6. Comparison of changes in fluid load support (FLS), articular tensile strain (E_1) and osteochondral shear stress (τ_{max}) during (A) single-leg stance from initial loading to 600 s, (B) gait over 10 cycles and (C) squatting over 10 cycles. FLS decreased by less than 5% from baseline during the simulated activities of 600 s of SLS and 10 cycles of gait and squatting. The removal of the labrum resulted in decreased relaxation of E_1 and τ_{max} during SLS. During gait and squatting, the differences were negligible. The elastic model experienced no changes in FLS, E_1, or τ_{max} during SLS, and experienced negligible changes during peak loading of gait and squatting cycles.

should be roughly two orders of magnitude lower than that computed using Eq. (1).

Several studies emphasize the importance of the labrum in sealing fluid within the intra-articular space (Cadet et al., 2012; Dwyer et al., 2014; Ferguson et al., 2000a,b, 2003; Philippon et al., 2014), but the influence of the labrum on fluid pressurization within the articular cartilage itself has not been studied. Although it has been shown in both computational (Ferguson et al., 2000a, 2000b) and experimental studies (Dwyer et al., 2015; Dwyer et al., 2014; Ferguson et al., 2003; Philippon et al., 2014) that the labrum helps maintain intra-articular fluid pressure within the joint space of the hip, this may not directly translate to maintenance of fluid pressure in the cartilage layer due to the discrepancy in magnitudes. The magnitude of pressure within the joint space is reported between 20 and 500 kPa by experimental studies (Dwyer et al., 2015; Dwyer et al., 2014; Ferguson et al., 2003) (the wide range is primarily due to variations in protocol, especially applied loading scenario). This magnitude (kPa range) is small in contrast to the relatively high contact pressure (and therefore the fluid pressure due to the initial incompressibility) on the articular cartilage, which is reported around 4–14 MPa (Anderson et al., 2008; Anderson et al., 2010; Henak et al., 2014a; Henak et al., 2011), and predicted in the present study to be in this range. This order of magnitude difference implies that even when the intra-articular space is pressurized, fluid may flow out of the articular cartilage, resulting in loss of fluid load support. Taken together with the results of the current study, this suggests that the labrum plays a limited role in maintaining fluid pressurization within the articular cartilage itself.

In contrast to the lack of any significant effect of labrum removal on fluid pressurization within the articular cartilage, removal of the labrum resulted in increased displacement of the cartilage edge at the articular surface, which led to higher values

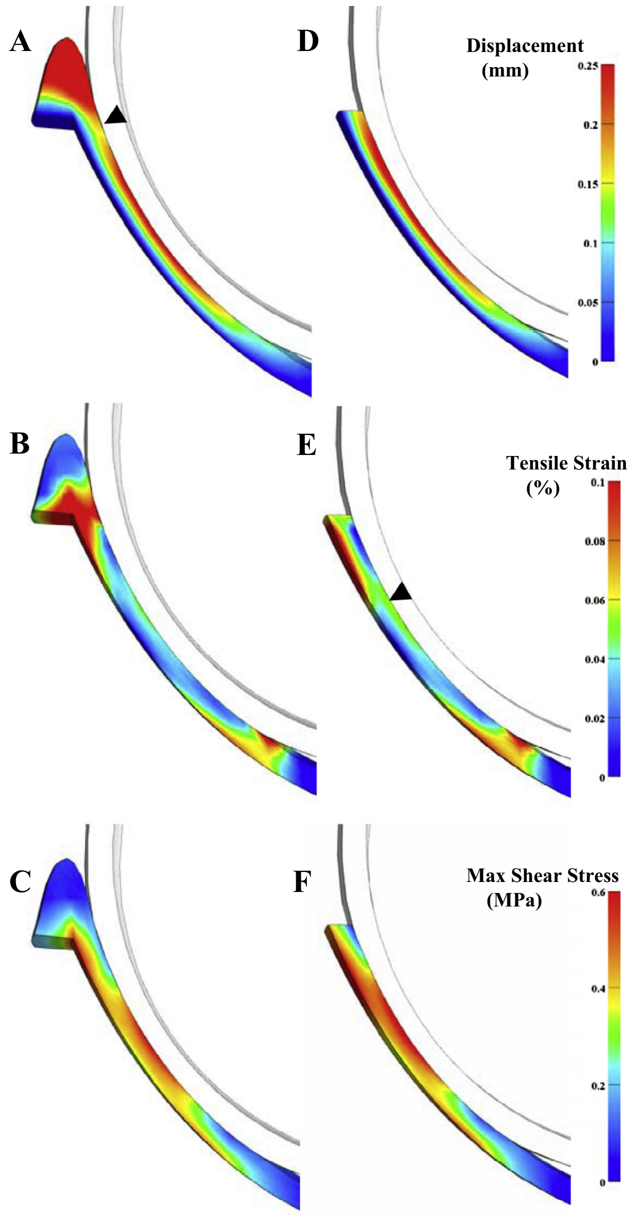

Fig. 7. Cross-sectional view of the acetabular cartilage during single-leg stance at 600 s for baseline and labrum removed cases. (A) When the labrum was intact, the applied load during single leg stance caused radial displacement of the labrum and resulted in (B and C) concentrated tensile strain and shear stress at the chondrolabral junction. (D) Removal of the labrum allowed slightly greater displacement at the edge of the articular cartilage than the intact model in the region marked by the arrow in A. (E) This caused increased tensile strain in the contact region of the articular surface, marked by an arrow, as well as (F) increased maximum shear stress at the osteochondral interface.

of E_1 and τ_{max} during SLS, and decreased relaxation of E_1 during gait and squatting. For completeness, changes in contact area were minimal between baseline and models with the labrum removed. Moreover, load supported by the labrum for baseline models was 0–2% during SLS and gait, and 0–4% for squatting, which is consistent with previous findings (Henak et al., 2014a; Henak et al., 2011). Further, although the labral load support for the baseline model was highest during the squatting condition, removal of the labrum resulted in the largest effect on stress and strain conditions during SLS. These data suggest the labrum is functioning as a mechanical boundary rather than as a seal for fluid within the cartilage layer. The free edge of the articular cartilage caused by the disrupted chondrolabral boundary may increase risk of damage. Currently, the major goals for labral repair are to restore native anatomy of the labrum and contact with the femoral head (Fry and Domb, 2010). Further investigation should assess if preservation strategies emphasizing labral reattachment to the acetabular rim of the cartilage edge to prevent deformation of the cartilage edge (without disrupting or with repair of the chondrolabral junction) may protect against conditions leading to chondral degradation.

We implemented several technical advances for modeling hip chondrolabral mechanics in this study. This was the first study to represent the articular cartilage in the hip with strain-dependent, anisotropic permeability, rather than constant and isotropic. Additionally, this is the first study to use a physiological transchondral fibril reinforcement defined using a gradient between zones to scale the contributions from the continuous fiber distribution model throughout the layer. This is in contrast to other methods, for instance, which used distinct layers with orthogonal fibril reinforcement (Li et al., 2016). The final mesh included 7 layers of hexahedral elements through the thickness with biasing towards the articular and osteochondral surfaces, which is more refined than previous studies. Analysis focused on transchondral stress and strain, rather than contact stress, since the former are correlated to mechanical damage to articular cartilage in the hip. We used dynamic, time-dependent kinematics and load boundary conditions, rather than static positions during points of the cyclic activities. Finally, this was the first study to report simulation of the gait cycle for more than 10 cycles. This showed slight changes in the results, but steady-state was reached for the variables analyzed in about 60 cycles, or 65 s.

Inclusion of a physiological representation of collagen fibril orientation through the thickness of the cartilage was not necessary to accurately predict fluid load support. However, the predictions for the solid phase stress and strain fields were affected by idealized fiber orientations, which is similar to results for the knee (Mononen et al., 2012; Shirazi et al., 2008), and for articular cartilage generally (Meng et al., 2017). Fibril orientation perpendicular to the bony interface in the deep zone slightly decreased the maximum shear stress at this surface; since shear stress at this location is reported to cause delamination, this may protect against this type of damage. The fibril orientation in the superficial zone tangential to the surface allows the fibrils to bear more loading and reduce load to the matrix, since collagen fibrils only support load in tension. This configuration increased the tensile strain slightly at the articular surface. However, tensile strain at the surface may lead to fissuring and damage of the collagen fibrils; patients with osteoarthritis of the hip show decreased or no tangential fibrils in the superficial zones of the articular cartilage (Makela et al., 2012). These changes indicate that the physiological orientation plays at least a minor role in preserving the health of the cartilage in the hip.

Increasing the permeability for the articular cartilage increased rate of fluid exudation and, consequently, relaxation for E_1 and τ_{max}. Due to the wide range of permeability values reported in the literature, future studies should determine this parameter carefully.

The current study used an idealized, patient-based model of cartilage layers in the hip to ensure population-relevant geometry, to establish a well-defined parametric framework, and to decrease computational expense. The hip geometry from a patient was idealized to analyze the mechanics without the complexities of patient-specific geometry with potentially unique results specific to the individual. Further, parametric studies are much easier to conduct with well-defined geometry (e.g. constant cartilage thickness, simple geometry with a closed contact area). This approach allowed general conclusions to be made regarding the effects of the conditions studied. It may be useful for subsequent studies to investigate similar factors on additional models with common pathologies, especially in the context of cartilage defects. These analyses are computationally demanding; with the converged mesh, the model took approximately 1.5 h to run 600 s of SLS, 37 h to run 10 cycles of gait, and 21.5 h to run 10 cycles of squatting on a shared memory computer utilizing 16 Xeon X5550 cores and roughly 4 GB of core memory. We expect a patient-specific model would require additional refinement to adequately capture irregularities in geometry and would at least double the computational expense.

Several modeling assumptions that were used in the present study are worthy of discussion. A rigid representation of subchondral bone may overestimate stresses at the osteochondral interface and contact pressure compared to deformable bones, and increased congruency of the idealized model may underestimate contact pressure due to a larger contact area (Anderson et al., 2008). However, key findings were based on relative changes to variables measured, rather than their magnitude, and trends should still hold when applied to patient-specific models. Additionally, the effects of osmotic pressure were not considered, which have recently been shown to be an important factor in load dissipation and support most of the loading during equilibrium conditions (Quiroga et al., 2017). The additional consideration of osmotic pressure may decrease the magnitude of stress and strain conditions in the present study; however, since the FLS remains high throughout the analyzed motions in the present study, the results are within a range where we do not expect much load to be dissipated to osmotic swelling.

In conclusion, simulated cyclic motions of gait and squatting may be approximated with an elastic incompressible model without loss of accuracy due to fluid load support or flow-dependent viscoelasticity. Additionally, removal of the labrum only slightly decreased fluid load support within the articular cartilage, in contrast to the significant effect as a boundary for cartilage deformation. Further investigation should be conducted to assess if preservation strategies emphasizing labral reattachment to the acetabular rim would provide increased protection against chondral degradation.

Acknowledgements

The authors would like to acknowledge Brandon Zimmerman, Dave Rawlins, Lexie Floor, Nathan Galli, and David Zou for their contributions to this study. Funding was provided by the National Science Foundation Graduate Research Fellowship Program, the LS Peery Discovery Program in Musculoskeletal Restoration (Department of Orthopaedics, University of Utah), the University of Utah Seed Grant Program and NIH #R01GM083925. The funding agencies had no role in study design, data collection, analysis or interpretation, manuscript writing, or the decision to submit the manuscript.

Conflict of interest

The authors have no conflicts of interest.

Appendix A. Supplementary material

Supplementary Methods and Results, loading and kinematics data for gait and squatting, as well as a video displaying the simulated motions associated with this article can be found, in the online version, at https://doi.org/10.1016/j.jbiomech.2018.01.001.

References

Abraham, C.L., Bangerter, N.K., McGavin, L.S., Peters, C.L., Drew, A.J., Hanrahan, C.J., Anderson, A.E., 2015. Accuracy of 3D dual echo steady state (DESS) MR arthrography to quantify acetabular cartilage thickness. J. Magn. Reson. Imaging 42, 1329–1338.

Anderson, A.E., Ellis, B.J., Maas, S.A., Peters, C.L., Weiss, J.A., 2008. Validation of finite element predictions of cartilage contact pressure in the human hip joint. J. Biomech. Eng. 130, 051008.

Anderson, A.E., Ellis, B.J., Maas, S.A., Weiss, J.A., 2010. Effects of idealized joint geometry on finite element predictions of cartilage contact stresses in the hip. J. Biomech. 43, 1351–1357.

Ateshian, G.A., Ellis, B.J., Weiss, J.A., 2007. Equivalence between short-time biphasic and incompressible elastic material responses. J. Biomech. Eng. 129, 405–412.

Ateshian, G.A., Henak, C.R., Weiss, J.A., 2015. Toward patient-specific articular contact mechanics. J. Biomech. 48, 779–786.

Ateshian, G.A., Rajan, V., Chahine, N.O., Canal, C.E., Hung, C.T., 2009. Modeling the matrix of articular cartilage using a continuous fiber angular distribution predicts many observed phenomena. J. Biomech. Eng. 131, 061003.

Ateshian, G.A., Wang, H., 1995. A theoretical solution for the frictionless rolling contact of cylindrical biphasic articular cartilage layers. J. Biomech. 28, 1341–1355.

Athanasiou, K.A., Agarwal, A., Dzida, F.J., 1994. Comparative study of the intrinsic mechanical properties of the human acetabular and femoral head cartilage. J. Orthop. Res. 12, 340–349.

Bachrach, N.M., Mow, V.C., Guilak, F., 1998. Incompressibility of the solid matrix of articular cartilage under high hydrostatic pressures. J. Biomech. 31, 445–451.

Bader, D.L., Salter, D.M., Chowdhury, T.T., 2011. Biomechanical influence of cartilage homeostasis in health and disease. Arthritis 2011, 979032.

Beck, M., Kalhor, M., Leunig, M., Ganz, R., 2005. Hip morphology influences the pattern of damage to the acetabular cartilage: femoroacetabular impingement as a cause of early osteoarthritis of the hip. J. Bone Joint Surg. Br. 87, 1012–1018.

Bergmann, G., Deuretzbacher, G., Heller, M., Graichen, F., Rohlmann, A., Strauss, J., Duda, G.N., 2001. Hip contact forces and gait patterns from routine activities. J. Biomech. 34, 859–871.

Cadet, E.R., Chan, A.K., Vorys, G.C., Gardner, T., Yin, B., 2012. Investigation of the preservation of the fluid seal effect in the repaired, partially resected, and reconstructed acetabular labrum in a cadaveric hip model. Am. J. Sports Med. 40, 2218–2223.

Carter, D.R., Beaupre, G.S., 1999. Linear elastic and poroelastic models of cartilage can produce comparable stress results: a comment on Tanck et al. (J Biomech 32: 153-161, 1999). J. Biomech. 32, 1255–1256.

Carter, D.R., Beaupre, G.S., Wong, M., Smith, R.L., Andriacchi, T.P., Schurman, D.J., 2004. The mechanobiology of articular cartilage development and degeneration. Clin. Orthop. Relat. Res., S69–77

Chegini, S., Beck, M., Ferguson, S.J., 2009. The effects of impingement and dysplasia on stress distributions in the hip joint during sitting and walking: a finite element analysis. J. Orthop. Res. 27, 195–201.

Dagenais, S., Garbedian, S., Wai, E.K., 2009. Systematic review of the prevalence of radiographic primary hip osteoarthritis. Clin. Orthop. Relat. Res. 467, 623–637.

Demarteau, O., Pillet, L., Inaebnit, A., Borens, O., Quinn, T.M., 2006. Biomechanical characterization and in vitro mechanical injury of elderly human femoral head cartilage: comparison to adult bovine humeral head cartilage. Osteoarthritis Cartilage/OARS, Osteoarthritis Res. Soc. 14, 589–596.

Dwyer, M.K., Jones, H.L., Field, R.E., McCarthy, J.C., Noble, P.C., 2015. Femoroacetabular impingement negates the acetabular labral seal during pivoting maneuvers but not gait. Clin. Orthop. Relat. Res. 473, 602–607.

Dwyer, M.K., Jones, H.L., Hogan, M.G., Field, R.E., McCarthy, J.C., Noble, P.C., 2014. The acetabular labrum regulates fluid circulation of the hip joint during functional activities. Am. J. Sports Med. 42, 812–819.

Eberhardt, A.W., Keer, L.M., Lewis, J.L., Vithoontien, V., 1990. An analytical model of joint contact. J. Biomech. Eng. 112, 407–413.

Ferguson, S.J., Bryant, J.T., Ganz, R., Ito, K., 2000a. The acetabular labrum seal: a poroelastic finite element model. Clin. Biomech. (Bristol, Avon) 15, 463–468.

Ferguson, S.J., Bryant, J.T., Ganz, R., Ito, K., 2000b. The influence of the acetabular labrum on hip joint cartilage consolidation: a poroelastic finite element model. J. Biomech. 33, 953–960.

Ferguson, S.J., Bryant, J.T., Ganz, R., Ito, K., 2003. An in vitro investigation of the acetabular labral seal in hip joint mechanics. J. Biomech. 36, 171–178.

Ferguson, S.J., Bryant, J.T., Ito, K., 2001. The material properties of the bovine acetabular labrum. J. Orthop. Res. 19, 887–896.

Flachsmann, E.R., Broom, N.D., Oloyede, A., 1995. A biomechanical investigation of unconstrained shear failure of the osteochondral region under impact loading. Clin Biomech (Bristol, Avon) 10, 156–165.

Fry, R., Domb, B., 2010. Labral base refixation in the hip: rationale and technique for an anatomic approach to labral repair. Arthroscopy 26, S81–89.

Grodzinsky, A.J., Levenston, M.E., Jin, M., Frank, E.H., 2000. Cartilage tissue remodeling in response to mechanical forces. Annu. Rev. Biomed. Eng. 2, 691–713.

Guilak, F., 2011. Biomechanical factors in osteoarthritis. Best Pract. Res. Clin. Rheumatol. 25, 815–823.

Guilak, F., Fermor, B., Keefe, F.J., Kraus, V.B., Olson, S.A., Pisetsky, D.S., Setton, L.A., Weinberg, J.B., 2004. The role of biomechanics and inflammation in cartilage injury and repair. Clin. Orthop. Relat. Res., 17–26

Haemer, J.M., Carter, D.R., Giori, N.J., 2012. The low permeability of healthy meniscus and labrum limit articular cartilage consolidation and maintain fluid load support in the knee and hip. J. Biomech. 45, 1450–1456.

Harris, M.D., Anderson, A.E., Henak, C.R., Ellis, B.J., Peters, C.L., Weiss, J.A., 2012. Finite element prediction of cartilage contact stresses in normal human hips. J. Orthop. Res. 30, 1133–1139.

Hayes, W.C., Keer, L.M., Herrmann, G., Mockros, L.F., 1972. A mathematical analysis for indentation tests of articular cartilage. J. Biomech. 5, 541–551.

Henak, C.R., Abraham, C.L., Anderson, A.E., Maas, S.A., Ellis, B.J., Peters, C.L., Weiss, J. A., 2014a. Patient-specific analysis of cartilage and labrum mechanics in human hips with acetabular dysplasia. Osteoarthritis Cartilage 22, 210–217.

Henak, C.R., Ateshian, G.A., Weiss, J.A., 2014b. Finite element prediction of transchondral stress and strain in the human hip. J. Biomech. Eng. 136, 021021.

Henak, C.R., Ellis, B.J., Harris, M.D., Anderson, A.E., Peters, C.L., Weiss, J.A., 2011. Role of the acetabular labrum in load support across the hip joint. J. Biomech. 44, 2201–2206.

Holmes, M.H., Mow, V.C., 1990. The nonlinear characteristics of soft gels and hydrated connective tissues in ultrafiltration. J. Biomech. 23, 1145–1156.

Huang, C.Y., Mow, V.C., Ateshian, G.A., 2001. The role of flow-independent viscoelasticity in the biphasic tensile and compressive responses of articular cartilage. J. Biomech. Eng. 123, 410–417.

Klennert, B.J., Ellis, B.J., Maak, T.G., Kapron, A.L., Weiss, J.A., 2017. The mechanics of focal chondral defects in the hip. J. Biomech. 52, 31–37.

Li, J., Hua, X., Jin, Z., Fisher, J., Wilcox, R.K., 2014. Biphasic investigation of contact mechanics in natural human hips during activities. Proc. Inst. Mech. Eng. H 228, 556–563.

Li, J., Hua, X., Jones, A.C., Williams, S., Jin, Z., Fisher, J., Wilcox, R.K., 2016. The influence of the representation of collagen fibre organisation on the cartilage contact mechanics of the hip joint. J. Biomech. 49, 1679–1685.

Li, J., Stewart, T.D., Jin, Z., Wilcox, R.K., Fisher, J., 2013. The influence of size, clearance, cartilage properties, thickness and hemiarthroplasty on the contact mechanics of the hip joint with biphasic layers. J. Biomech. 46, 1641–1647.

Liu, L., Ecker, T.M., Schumann, S., Siebenrock, K.A., Zheng, G., 2016. Evaluation of constant thickness cartilage models vs. patient specific cartilage models for an optimized computer-assisted planning of periacetabular osteotomy. PLoS One 11, e0146452.

Maas, S.A., Ellis, B.J., Rawlins, D.S., Weiss, J.A., 2016. Finite element simulation of articular contact mechanics with quadratic tetrahedral elements. J. Biomech. 49, 659–667.

Macirowski, T., Tepic, S., Mann, R.W., 1994. Cartilage stresses in the human hip joint. J. Biomech. Eng. 116, 10–18.

Makela, J.T., Huttu, M.R., Korhonen, R.K., 2012. Structure-function relationships in osteoarthritic human hip joint articular cartilage. Osteoarthritis Cartilage 20, 1268–1277.

Mankin, H.J., 1974. The reaction of articular cartilage to injury and osteoarthritis (first of two parts). N. Engl. J. Med. 291, 1285–1292.

Meng, Q., An, S., Damion, R.A., Jin, Z., Wilcox, R., Fisher, J., Jones, A., 2017. The effect of collagen fibril orientation on the biphasic mechanics of articular cartilage. J. Mech. Behav. Biomed. Mater. 65, 439–453.

Minns, R.J., Steven, F.S., 1977. The collagen fibril organization in human articular cartilage. J. Anat. 123, 437–457.

Mononen, M.E., Mikkola, M.T., Julkunen, P., Ojala, R., Nieminen, M.T., Jurvelin, J.S., Korhonen, R.K., 2012. Effect of superficial collagen patterns and fibrillation of femoral articular cartilage on knee joint mechanics-a 3D finite element analysis. J. Biomech. 45, 579–587.

Mow, V.C., Kuei, S.C., Lai, W.M., Armstrong, C.G., 1980. Biphasic creep and stress relaxation of articular cartilage in compression? Theory and experiments. J. Biomech. Eng. 102, 73–84.

Mow, V.C., Lai, W.M., 1980. Recent developments in synovial joint biomechanics. SIAM Rev. 22, 275–317.

Park, S., Hung, C.T., Ateshian, G.A., 2004. Mechanical response of bovine articular cartilage under dynamic unconfined compression loading at physiological stress levels. Osteoarthritis Cartilage 12, 65–73.

Pawaskar, S.S., Ingham, E., Fisher, J., Jin, Z., 2011. Fluid load support and contact mechanics of hemiarthroplasty in the natural hip joint. Med. Eng. Phys. 33, 96–105.

Pawaskar, S.S., Jin, Z.M., Fisher, J., 2007. Modelling of fluid support inside articular cartilage during sliding. P I Mech. Eng. J-J. Eng. 221. 455-455.

Philippon, M.J., Nepple, J.J., Campbell, K.J., Dornan, G.J., Jansson, K.S., LaPrade, R.F., Wijdicks, C.A., 2014. The hip fluid seal–Part I: the effect of an acetabular labral tear, repair, resection, and reconstruction on hip fluid pressurization. Knee Surg. Sports Traumatol. Arthrosc. 22, 722–729.

Quapp, K.M., Weiss, J.A., 1998. Material characterization of human medial collateral ligament. J. Biomech. Eng. 120, 757–763.

Quiroga, J.M., Wilson, W., Ito, K., van Donkelaar, C.C., 2017. Relative contribution of articular cartilage's constitutive components to load support depending on strain rate. Biomech. Model. Mechanobiol. 16, 151–158.

Reynaud, B., Quinn, T.M., 2006. Anisotropic hydraulic permeability in compressed articular cartilage. J. Biomech. 39, 131–137.

Shepherd, D.E., Seedhom, B.B., 1999. Thickness of human articular cartilage in joints of the lower limb. Ann. Rheum. Dis. 58, 27–34.

Shirazi, R., Shirazi-Adl, A., Hurtig, M., 2008. Role of cartilage collagen fibrils networks in knee joint biomechanics under compression. J. Biomech. 41, 3340–3348.

Wu, J.Z., Herzog, W., 2000. Finite element simulation of location- and time-dependent mechanical behavior of chondrocytes in unconfined compression tests. Ann. Biomed. Eng. 28, 318–330.